A 3D model of a reverse vortex flow gliding arc reactor

3D model of a reverse vortex flow gliding arc reactor

G Trenchev[1], St Kolev[2] and A Bogaerts[1]

[1]Research group PLASMANT, Department of Chemistry, University of Antwerp, Universiteitsplein 1, B-2610 Antwerp, Belgium
[2]Faculty of Physics, Sofia University, 5 James Bourchier Boulevard, 1164 Sofia, Bulgaria

E-Mail: georgi.trenchev@uantwerpen.be

Abstract. In this computational study, a gliding arc plasma reactor with a reverse-vortex flow stabilization is modelled for the first time by means of a fluid plasma description. The plasma reactor is operating with argon gas at atmospheric pressure. The gas flow is simulated using the k-ε RANS turbulent model. A quasi-neutral fluid plasma model is employed for computing the plasma properties. The plasma arc movement in the reactor is observed, and the results for the gas flow, electrical characteristics, plasma density, electron temperature, and gas temperature are analyzed.

PACS: 52.50.Dg, 52.50.Nr, 52.65.Kj, 52.80.Mg

Keywords: gliding arc, argon plasma, atmospheric pressure, 3D, fluid modelling, vortex flow

1. Introduction

Gliding arc (GA) plasma reactors are atmospheric plasma sources characterized by simplicity and reliability [1]. They are non-thermal reactors operating at a typically high electron temperature (above 1 eV), high plasma density (in the order of 10^{20} - 10^{22} m^{-3}), and a moderate gas temperature (1000 - 3000 K) [1, 2, 3, 4].

The well-known conventional GA is a non-stationary atmospheric plasma reactor consisting of two or more blade-shaped electrodes, between which a high voltage is applied. The arc is self-initiated at the narrowest gap between the electrodes, where the gas enters the reactor. Then the arc travels through the reactor forced by the gas flow and convection. When the distance between the electrodes becomes too large for the arc to sustain, it extinguishes, and a new arc is initiated at the narrowest gap, forming a consistent, iterative operation of the device.

GA plasma reactors are recently gaining increasing interest for CO_2 conversion into value-added chemicals and new fuels [5, 6, 7, 8, 9]. While conventional GA reactors give already reasonable results, they suffer from a couple of important problems. GA reactors deteriorate due to strong electrode degradation as a result of the high current density of the discharge. Moreover, as the electrodes are usually quite thin, a significant amount of gas passes past the plasma without being converted, which limits the gas conversion efficiency [8, 10]. With these concerns in mind, improved designs are constantly sought.

The newly envisaged technique of vortex flow stabilization allows for lower heat losses of the plasma in the GA [1, 10]. Furthermore, it improves the electrode lifetime, the ionization efficiency and the gas conversion [9]. A forward-vortex flow (FVF) stabilized GA reactor consists of a cylindrical tube with a swirl generator, mounted on the opposite side with respect to the axial gas outlet. The swirl generator usually contains four or more tangentially oriented inlets. The tangentially applied gas stream initiates a vortex swirl flow along the walls of the tube, partially isolating the plasma from the walls, and lowering its heat loss, thus improving the reactor efficiency.

A more efficient way of vortex plasma stabilization is the reverse-vortex flow (RVF) [9, 10, 13]. In this configuration, the swirl generator is on the same side as the gas outlet. The result is a secondary, backwards oriented inner vortex stream within the outer tangential flow along the walls. The plasma itself is confined within the inner flow, providing nearly perfect heat insulation from the walls, which leads to an even higher degree of ionization, and a higher energy efficiency [10, 11]. Moreover, the RVF leads to better gas mixing, which further improves the gas conversion [9]. These advantages are crucial for applications involving gas reforming and conversion, where the energy efficiency determines the overall applicability of the device. The RVF stabilization has also been applied successfully for other types of atmospheric discharges, such as microwave [13], inductively coupled plasma [14] and for gaseous flames [15]. The RVF configuration in the reactor under study will be described in detail in Section 2 below.

A number of experiments and numerical simulations have been conducted in order to evaluate the operating characteristics of the RVF GA plasma reactor. Kalra et al. investigated some properties of the RVF GA reactor through experiments [10, 13]. DC discharge plasmas with RVF stabilization were also investigated by Nedybaliuk et al. [12]. A high CO_2 conversion efficiency was achieved using a GA in a tornado flow [7]. Furthermore, Gutsol and Bakken investigated a RVF plasma reactor, albeit not for a GA but for a microwave plasma, through experiments and computer simulations, and compared it to its FVF variant, concluding a significantly lower heat loss at the walls for the more advanced RVF reactor [11]. Although the RVF GA reactor shows very promising results, the underlying mechanisms are still far from understood. Computational models describing the plasma properties in such a reactor are sparse, and often, very limited. A better understanding through plasma modelling would be beneficial both from fundamental point of view and for real-world applications.

In the present paper, we present a 3D computational model of the GA in RVF configuration, developed by means of the Comsol Multiphysics simulation software. Modelling plasma in 3D requires a very sophisticated approach, as the available computing power represents a serious limitation. Previous work pointed out that a complete fluid plasma model for a GA in 3D is simply unrealistic [16]. Therefore, certain reductions are made to the present model, such as the plasma quasi-neutrality assumption and a reduction of the chemistry set and number of species. Despite these simplifications, and given the challenge of modelling plasma in 3D, we expect the model to reasonably cover the scope of the study.

In section 2, the model will be described in detail, starting with the gas flow simulation and the corresponding geometry, equations, parameters and boundary conditions. Next, the quasi-neutral model will be mathematically described, clarifying the significance of the reductions and simplifications. The chemistry reaction set will also be provided, followed by an equivalent electrical scheme of the model.

Section 3 starts with results of the gas flow simulation with detailed streamlines, velocity and pressure plots, explaining the formation of a RVF. Subsequently, the results for the electrical properties of the plasma arc, such as voltage, current and current density, will be presented. The model is computed for different gas flow rates and cathode currents. Finally, the basic plasma characteristics, such as the plasma density, electron temperature and gas temperature, will be provided.

In the last section, final conclusions on this study will be given. The results will be discussed both from a fundamental point of view, and within the scope of the real-world applicability of the method. Some remarks on the model performance will be given as well.

2. Model description

2.1. Gas flow model

The model uses a simplified geometry, which is shown in figure 1, along with its finite – element mesh in figure 2. A cylinder with a radius of 6 mm and a height of 5 mm represents the plasma chamber. There are 4 tangential gas inlets, each with radius of 0.8 mm, and one axial outlet at the top, with radius of 2.5 mm. All chamber edges are smooth in order to prevent strong velocity gradients and turbulent eddies. This geometry is based on the RVF gliding arc reactor concept presented in [1].

The gas flow rate ranges from 20 to 50 L/min in the model. The velocity magnitudes go up to 300 m/s inside the reactor, suggesting a highly turbulent gas flow.

In fluid and gas flows, turbulence stands for rapid oscillations of velocity and pressure, varying over a wide range both in space and time. Contrary to laminar flows, which are quite predictive, turbulent flows are much more chaotic in nature, requiring a greater amount of computing power to be solved numerically.

Gas flow models are usually based on solving the Navier-Stokes equations by means of a discretization mesh [17]. As the flow speed increases, so does the level of turbulence in the flow, resulting in more frequent and denser turbulent oscillating eddies, which requires a smaller finite mesh in order to obtain a solution. Such computation is beyond reach, even for modern workstation computer systems. In fact, solving turbulent flows in 3D using the Navier-Stokes equations in their full form still requires supercomputer facilities.

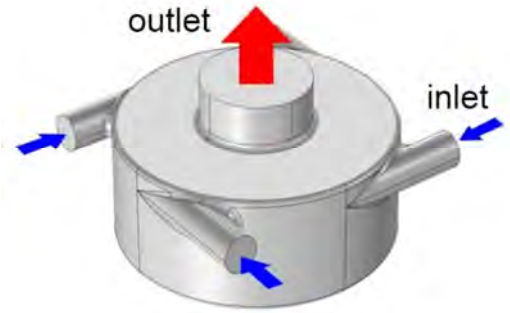

Figure 1. RVF gliding arc reactor geometry.

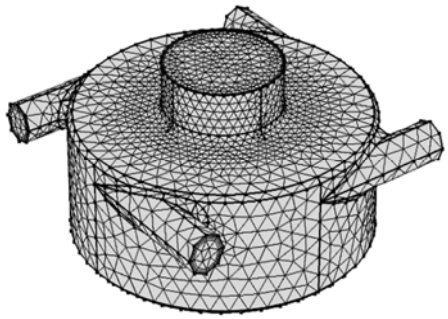

Figure 2. RVF gliding arc reactor finite element mesh.

Combined with the plasma model itself, it is clear that this approach would drastically exceed the available computational resources. For this reason, the gas flow is simulated using the so-called k-ε Reynolds-averaged-Navier-Stokes (RANS) turbulent modelling technique, which effectively averages all fluctuating turbulent quantities over time, greatly reducing the computational cost [17, 18].

The following Navier-Stokes equations for Newtonian fluid (mass continuity and momentum continuity) are solved for the fluid flow model:

$$\nabla.\left(\rho\overrightarrow{u_g}\right) = 0 \tag{1}$$

$$\rho\left(\overrightarrow{u_g}.\nabla\right)\overrightarrow{u_g} = \nabla.\left[-p\vec{I} + (\mu+\mu_{Tu})\left(\nabla\overrightarrow{u_g} + \nabla\left(\overrightarrow{u_g}\right)^T\right) - \frac{2}{3}(\mu+\mu_{Tu})\left(\nabla.\overrightarrow{u_g}\right)\vec{I} - \frac{2}{3}\rho k_{Tu}\vec{I}\right] + \vec{F} \tag{2}$$

where ρ stands for the gas density, $\overrightarrow{u_g}$ is the gas flow velocity vector, superscript T stands for transposition, p is the gas pressure, μ is the dynamic viscosity of the fluid, μ_{Tu} is the turbulent viscosity of the fluid, k_{Tu} is the turbulent kinetic energy, $\vec{I}$ is the unity tensor and $\vec{F}$ is the body force vector. Equation 1 and 2 are coupled with two more transport equations describing k_{Tu} and the

turbulent dissipation rate ε. As for the boundary conditions, the inlets (figure 1) are defined as gas flow normal velocity boundaries, and the outlet is defined as a zero-gradient outflow boundary. All walls permit no flux and conform the no-slip condition. Consequently, the RANS model should compute the flow vector in detail, representing the flow field, which would usually contain small turbulent oscillations (eddies) as a time-averaged quantity. The final solution is the gas flow velocity. This method is usually considered to be accurate for most engineering applications [19].

Besides the mass and momentum continuity equations, also the heat equation for the gas thermal balance needs to be solved, which reads as follows:

$$\rho C_p \frac{\partial T_g}{\partial t} + \rho C_p \overrightarrow{u_g} \cdot \nabla T_g - \nabla \cdot \left(k_g \nabla T_g \right) = Q \tag{3}$$

where ρ is the gas density, C_p is the heat capacity of the gas, k_g is the temperature-dependent gas thermal conductivity (based on a material look-up table), T_g is the gas temperature and Q accounts for the gas heating due to elastic and inelastic collisions between electrons and heavy particles in the plasma. In order to reduce the computation time, the gas flow model was solved first as a stationary problem and the obtained velocity field and turbulent energy dissipation were used in the plasma model coupled with the gas heating (eq. 3). Thus, the model does not consider the hydrodynamic influence of the gliding arc on the gas flow.

The model was computed within its full geometry with nearly 150,000 tetrahedral elements in the complete mesh, with element sizes ranging from 0.3 to 0.7 mm (see figure 2). The mesh is denser near the outlet, where the plasma arc is observed.

2.2. Quasi-neutral plasma model

Modelling atmospheric plasmas in 3D is a very challenging task. Often these models consider a discharge at thermal equilibrium, where the gas temperature and electron temperature are equal [20]. However, the GA exhibits a very complicated structure and behavior, including equilibrium and non-equilibrium stages, arc decay and re-ignition, and a complex arc body [21]. A thermal model would not provide the important plasma parameters for the given problem. On the other hand, describing the plasma using a complete fluid model in 3D would require a very long computational time [16]. In particular, the Debye sheaths formed at the cathode and the anode of the reactor present a significant problem, as they require a very fine finite element mesh (in the order of micrometers) to be solved correctly. For this reason, we have developed a simplified quasi-neutral model, where the ion and electron densities are equal, and thus no Debye sheath can be formed. This approach was recently evaluated for a classical GA, with very satisfying results, concluding that the sheath process has no significant influence on the final solution for the arc column [22]. The quasi-neutral model simultaneously solves the equations for the plasma density, electron and gas temperature and electric fields as a function of time.

The initial streamer stage of the arc is omitted, as it requires additional modelling effort. Instead, an artificial plasma heating function is induced at the initial arc position, creating a temporary plasma channel for the arc to ignite. Once the arc is initiated, the artificial heating is cut-off, leaving the arc to be sustained only by the electric current flowing through the plasma. The streamer stage of an atmospheric discharge is a very short process in the order of nanoseconds, and should not influence the operating properties of the GA reactor [1].

In figures 3 and 4, the plasma heating function shape in the reactor and its time dependence are plotted. The function has a maximum at 9.5×10^{-6} s, and is completely cut-off after 1.05×10^{-5} s. Applying this artificial plasma heating function does not influence the obtained results. Indeed, numerical tests showed that the arc characteristics after 100 μs do not depend on the initial breakdown process, provided that it is considerably shorter (10 times here) and it does not deposit considerable

amount of energy (much lower than the arc energy deposition). The total amount of energy deposited by the artificial heating function amounts to 10^{-6} J, while the actual arc deposits 0.01 J for 100 µs, when the arc is already independent from the heating function.

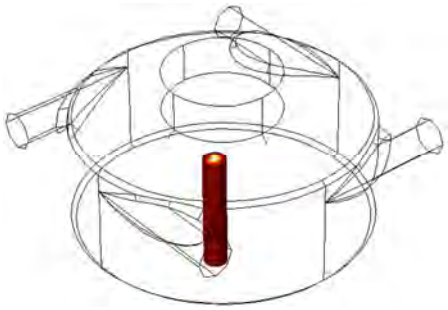

Figure 3. Artificial heat function shape – a straight column with a Gaussian distribution (2D Gaussian in the x-y plane and uniform along z) of the power density.

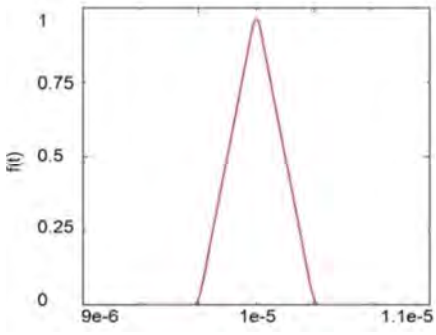

Figure 4. Artificial heat function over time.

To further limit the calculation time of the model, the chemistry reaction set is significantly reduced compared to what is mostly used with argon discharge modelling [16]. Only one type of ions and one type of excited species are considered. The mathematical description of the model is based on [23] and [24], and is presented below.

Assuming the drift-diffusion approximation, we start with the electron balance equation, which reads:

$$\frac{\partial n_e}{\partial t} + \nabla.\left(-D_e\nabla n_e - \mu_e n_e\overrightarrow{E_{amb}}\right) + \left(\vec{u}_g.\nabla\right)n_e = R_e \tag{4}$$

In analogy, the ion balance equation is as follows:

$$\frac{\partial n_i}{\partial t} + \nabla.\left(-D_i\nabla n_i + \mu_i n_i\overrightarrow{E_{amb}}\right) + \left(\vec{u}_g.\nabla\right)n_i = R_i \tag{5}$$

where n_e and n_i stand for the electron and ion density, respectively, μ_e and μ_i stand for the electron and ion mobility, respectively, $\overrightarrow{E_{amb}}$ is the ambipolar electric field, $\vec{u}_g$ is the gas flow velocity vector, D_e and D_i stand for the electron and ion diffusion coefficients, and R_e and R_i stand for the electron and ion production and loss rates due to chemical reactions. The thermal diffusion of electrons is neglected in this case.

Assuming quasi-neutrality for the model, i.e. $n_e = n_i$ and equality of the fluxes, the ambipolar electric field can be derived as follows:

$$\overrightarrow{E_{amb}} = \frac{\nabla n_i(-D_e + D_i)}{n_i(\mu_i + \mu_e)} \tag{6}$$

The continuity equation for the excited species is the following:

$$\frac{\partial n_*}{\partial t} + \nabla.\left(D_*\nabla n_*\right) = R_* \tag{7}$$

where n_* and D_* stand for the species density and diffusion coefficient, respectively, and R_* is the corresponding source term. The convection term for the excited species is neglected, as their average life-time (in the order of nanoseconds) is very low compared to the movement speed of the arc, and therefore it does not influence the results.

The electron energy balance equation is solved as follows:

$$\frac{\partial n_e \bar{\varepsilon}_e}{\partial t} + \nabla.\left(-\mu_{\varepsilon,e} n_e \overrightarrow{E_{amb}} - D_{\varepsilon,e} \nabla(n_e \bar{\varepsilon}_e)\right) + \left(\vec{u}_g.\nabla\right) n_e \bar{\varepsilon}_e = \sigma_{pl} E^2 + n_e \Delta \bar{\varepsilon}_e + Q \qquad (8)$$

where $\bar{\varepsilon}_e$ is the averaged electron energy, σ_{pl} is the plasma conductivity (see below), E_{amb} is the absolute value of the ambipolar electric field, Q is the background heat source, and:

$$\mu_{\varepsilon,e} = \frac{5}{3}\mu_e \quad (9.1) \qquad\qquad D_{\varepsilon,e} = \frac{2}{3}\mu_{\varepsilon,e}\bar{\varepsilon}_e \quad (9.2)$$

where the terms $\mu_{\varepsilon,e}$ and $D_{\varepsilon,e}$ stand for the energy mobility and diffusion, respectively.

Instead of solving the Poisson equation, the electric field is derived from the law for current conservation:

$$\nabla.\left[\sigma_{pl}(-\nabla\varphi)\right] = 0 \qquad (10)$$

where φ is the electric potential, and the plasma conductivity (σ_{pl}) is solved as:

$$\sigma_{pl} = |q_e|(\mu_e n_e + \mu_i n_i) \qquad (11)$$

$with\ q_e$ being the electron charge. The electric field E is produced by the application of electric potential at the electrodes. The plasma heating and the electron temperature are a result of the applied electric field, however, the particle motion due to the electric field is not considered. In addition, no particle flux is permitted at boundary areas. Finally, the reduced set of electron collisions is given in Table 1:

Table1. Electron impact reaction set assumed in the model, with the references where the rate coefficients are adopted from.

Reaction	Rate coefficient	Ref.
$\boldsymbol{e + Ar \rightarrow e + Ar}$	BS[a]	[26]
$\boldsymbol{e + Ar \rightarrow e + Ar(4s)}$	BS	[26]
$\boldsymbol{e + Ar(4s) \rightarrow 2e + Ar^+}$	BS	[26]
$\boldsymbol{Ar^+ + e + Ar \rightarrow Ar + Ar}$	$k\left(m^6/s\right) = 1.5 \times 10^{-40}\left(\frac{T_g}{300}\right)^{-2.5}$ [b]	[16]

[a]Boltzmann solver, [b]T_g in K

2.3. Electrical circuit

The scheme in figure 5 represents the electrical circuit of the GA RVF reactor. The bottom boundary (see also figure 1) of the reactor is the cathode, connected to a ballast resistor, which in turn is connected to a voltage source supplying 1000V. The boundary at the top (see also figure 1), where the outlet is located, is the anode, or the grounded electrode. Such a configuration represents a flat-type

electrode RVF reactor. The current is limited by a ballast resistor (Rb), and a 100 pF capacitor (Cb) forms an RC filtering circuit. The total current for the system is varied by changing the value for the ballast resistor.

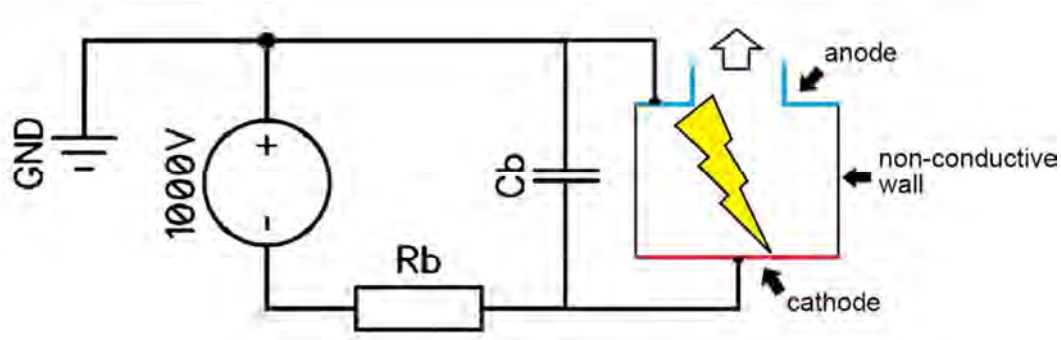

Figure 5. Representative electrical scheme of the GA reactor.

2.4. Boundary conditions

The boundary conditions implemented in the model are represented below. The model is structured in several computational interfaces in Comsol [25], each describing a different physical process, but sharing common variables. The Navier-Stokes equations (1, 2) are solved by the Fluid Flow interface. The equations governing particle flux and density (5, 7), electron energy balance (8, 9), the gas heat balance equation (3) and the current conservation equation (10) are implemented through the Mathematics interface. Eq. (4) is not computed because the electron density is assumed to be equal to the ion density in this quasi-neutral model. The reactor walls do not permit heat conduction, i.e. they act as insulators and their thermal balance is not considered. This is an approximation of the model, which we had to apply, mainly because of computational limitations The reactor outlet permits convective heat flux only. An additional differential equation solves for the electrical circuit (figure 5). As is the case with flows under high rotation, a significant reverse back-flow can be expected at the reactor outlet. In practice, this flow is suppressed by the buoyancy force caused by the hot gas. However, we do not consider the buoyancy force in the model. Therefore, the back-flow is suppressed in our model by the according boundary condition in table 2. The final solution for the plasma is derived as a multiphysics compilation.

Table 2. Boundary conditions implemented in the model.

Boundary	Expression	Equation	Description
Walls	$-\vec{n}\cdot\left(-D_i\nabla n_i-\mu_i n_i\overrightarrow{E_{amb}}\right)=0$	5	Zero flux
Walls	$-\vec{n}\cdot\left(-\mu_{\varepsilon,e}n_e\overrightarrow{E_{amb}}-D_{\varepsilon,e}\nabla(n_e\bar{\varepsilon}_e)\right)=0$	8	Zero flux
Walls	$-\vec{n}\cdot(D_*\nabla n_*)=0$	7	Zero flux
Walls	$-\vec{n}\cdot\left(-k\nabla T_g\right)=0$	3	Adiabatic walls
Cathode	$U=1000V$	10	Fixed potential
Anode	$U=0V$	10	Fixed potential
Inlets	$\vec{u}=-u_0\vec{n}$	1, 2	Normal flow
Outlet	$\left[-p\vec{I}+(\mu+\mu_{Tu})\left(\nabla\overrightarrow{u_g}+\left(\nabla\overrightarrow{u_g}\right)^T\right)-\frac{2}{3}(\mu+\mu_{Tu})(\nabla.\overrightarrow{u_g})\vec{I}-\frac{2}{3}\rho k_{Tu}\vec{I}\right]\vec{n}=-\widehat{p_0}\vec{n}$ $-\widehat{p_0}\leq p_0$	1, 2	Pressure Suppress backflow
Inlets	$T_g=293.15\ K$	3	
Outlet	$-\vec{n}\cdot\left(-k\nabla T_g\right)=0$	3	Fixed temperature Outflow

$\vec{n}$ *is the normal vector*, $\vec{I}$ is the unity tensor, p_0 is the atmospheric pressure, $\widehat{p_0}$ *is the adjusted pressure*

3. Results

3.1. Gas flow pattern

The gas flow is computed as a stationary solution within Comsol. With 150,000 tetrahedral mesh elements, the velocity streamlines and the pressure gradient are accurate enough for the purpose of the present study.

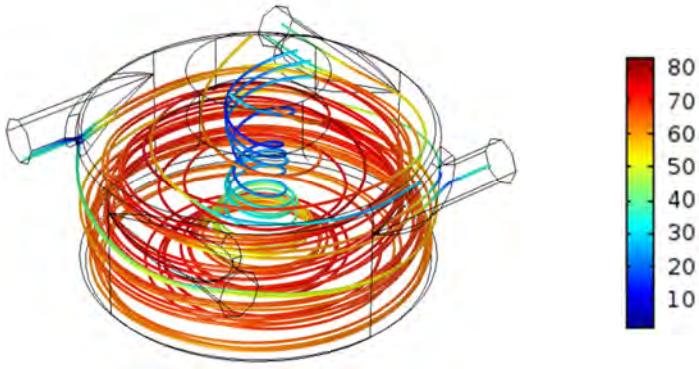

Figure 6. Gas velocity streamlines, for a flow rate of 22 L/min. Velocity magnitude (m/s)

In figure 6, the gas velocity streamlines are plotted in the 3D geometry. Notice the formation of a reverse-vortex in the middle, with lower velocity magnitude, leaving the reactor through the outlet. Figure 7 illustrates the values of the velocity in a vertical and horizontal cross section of the reactor. The flow velocity has its maximum value at the midpoint between the side walls and the reactor center. At the center, where the inner reverse-vortex is formed, the velocity is at minimum. Back-flows at the outlet are almost completely suppressed (see table 2).

As described before, the gas flow coming from the tangential inlets forms a high-velocity peripheral stream along the walls. The tangential inlets essentially act as a swirl generator. As the flow reaches the bottom of the reactor, a new vortex is formed in the reactor center (see figure 6). The inner vortex rotates in the same direction as the outer vortex, but travels in the opposite direction, i.e. in a reverse-vortex. Then the gas enters the reverse vortex area, leaving the reactor through the outlet at a low axial velocity.

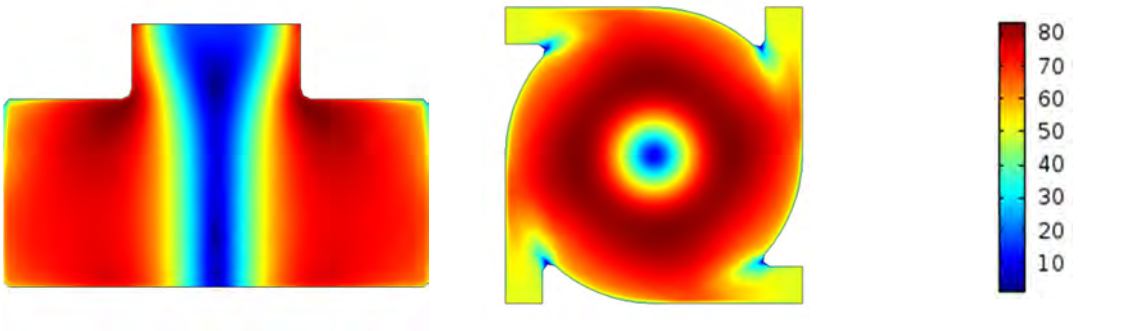

(a) (b) Velocity (m/s)

Figure 7. Gas velocity magnitude at a flow rate of 22 L/min (2D cross sections), cold flow.
(a) – vertical cross section (reactor center)
(b) – horizontal cross section (tangential inlets midpoint)

The gas becomes slightly pressurized along the side walls (with a pressure increase by about 17%) due to the high flow velocity (see figure 8). The inner vortex remains at relatively constant basic

pressure (1 atm.). The exit length (see figures 7-a and 8-a) may raise some questions regarding the correct application of the outlet boundary condition. However, a longer exit length does not influence the results.

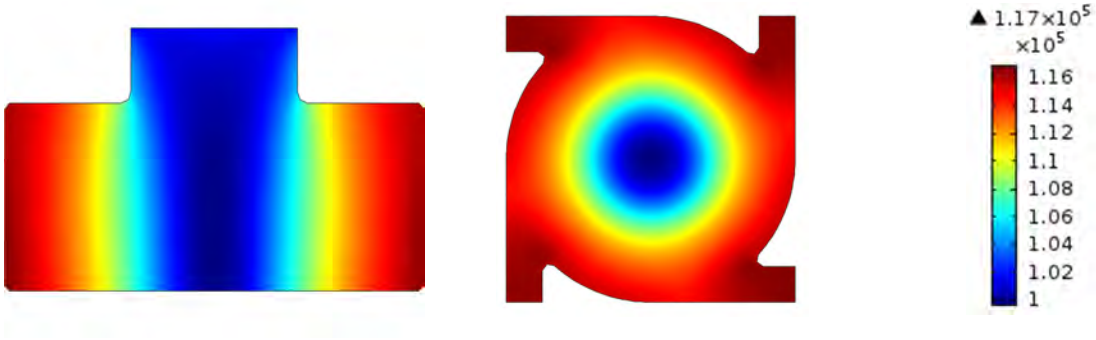

Figure 8. Gas pressure magnitude at a flow rate of 22 L/min (2D cross sections), cold flow.
(a) – vertical cross section (reactor center)
(b) – horizontal cross section (tangential inlets midpoint)

It is worth mentioning that the gas dynamics of a vortex flow are usually associated with the phenomenon of temperature separation between the inner and the outer vortex when the pressure drop in the system is significant (several bars). This process is called the Ranque effect, and the device itself is called a Ranque-Hilsch vortex tube [27]. In general, the reverse-vortex in this tube should have a lower temperature (usually about 50 K lower) than the outer peripheral vortex, essentially forming a cooling device without any moving parts. However, the used k-ε RANS description of the flow is not completely adequate for modelling this process. Moreover, the Ranque cooling effect should not significantly affect the plasma properties. Currently, the Ranque effect has no rigorous physical explanation, and is a subject of investigation [27]. Therefore, it is not discussed further, as it is also outside the scope of this study.

3.2. Plasma arc electrical properties

The gliding arc current is limited by the ballast resistor in the electrical circuit and the conductivity of the plasma channel. At the finite element mesh settings mentioned above, it takes about 48 hours on an Intel i7-3820 CPU to compute just 300 microseconds, or about 1 revolution for the arc in the reactor. The model calculates up to 1 millisecond. The plasma parameters remain stable over this time frame.

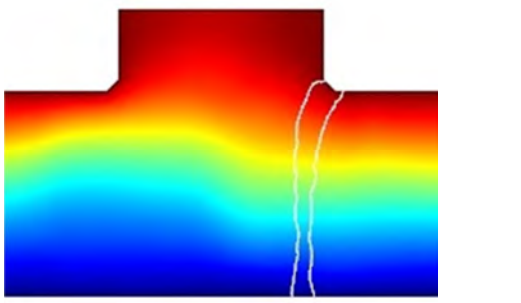

Figure 9. Electric potential distribution on a 2D cross-section of the reactor, at a cathode current of 900 mA and flow rate of 22 L/min, t = 200 µs. The arc body is indicated with white lines.

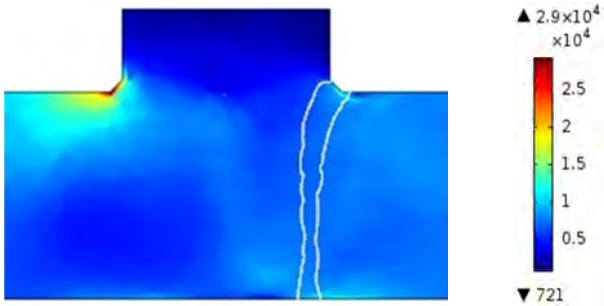

Figure 10. Electric field magnitude distribution on a 2D cross-section of the reactor, at a cathode current of 900 mA and flow rate of 22 L/min, t = 200 µs. The arc body is indicated with white lines.

In figure 9, on a centered cross-section of the reactor, the electric potential distribution is shown at a time of 1 ms, and it is visibly distorted by the plasma arc. Due to the curvature of the outlet edge, the electric field is stronger at the anode, as shown in figure 10. The arc ignites and rotates along this edge, as the discharge would normally take place between the points of highest electric field. As also seen in figure 10, the electric field is lower at the arc attachment spot due to the flowing electric current.

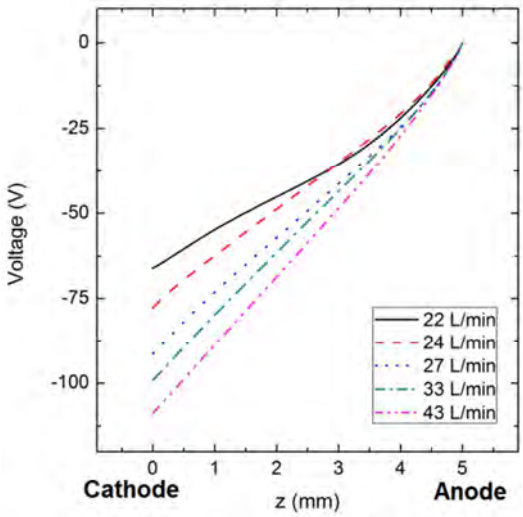

Figure 11. Axial plot of potential difference between anode and cathode at different flow rates. Rb = 1000 Ohm, t = 200 µs.

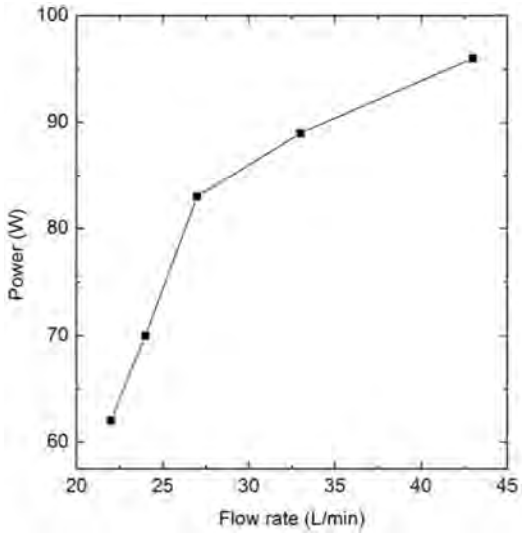

Figure 12. Reactor power consumption at different flow rates. Rb = 1000 Ohm, t = 200 µs.

GA discharges usually operate at a few tens to a few hundreds of volts after arc ignition, depending on the reactor dimensions and power [1, 3, 16]. Figure 11 illustrates the calculated voltage drop between the electrodes, as a function of axial position. The voltage is plotted for different gas flow rates. Position z = 0 corresponds to the cathode boundary, while z = 5 mm indicates the position of the anode boundary.

The potential difference between the electrodes after arc ignition (200 µs) at the lowest flow rate of 22 L/min is slightly above 60V, going up to 120V as the flow rate increases to 43 L/min. These voltage numbers exclude the sheath regions, as the model describes a quasi-neutral plasma. The higher potential difference also leads to higher power consumption in the reactor, as is clear from figure 12. The major reason for the arc voltage to increase with higher gas flow is the faster gas exchange, which lowers the arc gas temperature and thus increases its electrical resistance. At higher flow rates, the arc is also subjected to an increased convective cooling as a result of the higher axial gas flow in the reactor center.

The peak plasma conductivity σ_{pl} at the arc center (see equation 11) ranges between 100 and 150 S/m after arc ignition. As far as the model accuracy allows, it remains relatively constant for different gas flow rates and cathode currents.

In figures 13 and 14, the cathode current I and the peak arc current density J_{max} (at the arc center) are plotted as a function of ballast resistance and gas flow rate, respectively. The total cathode current drops accordingly with increasing ballast resistance (see figure 13), and the peak arc current density ranges between 1.10^6 and 3.10^6 A/m^2, which is a typical value for arc and gliding arc discharges [1, 4]. As noted above, higher flow rates cause higher arc electrical resistance, but the total cathode current and the peak arc current density remain nearly unchanged, with values around 900 – 950 mA and $2.5x10^6$ – $4x10^6$ A/m^2, respectively (see figure 14). The peak plasma density of the arc itself also remains constant with values in the range of 10^{21} m^{-3} (see section 3.3 below). The oscillations in the values for J_{max} could be due to numerical inaccuracies and mesh limitations.

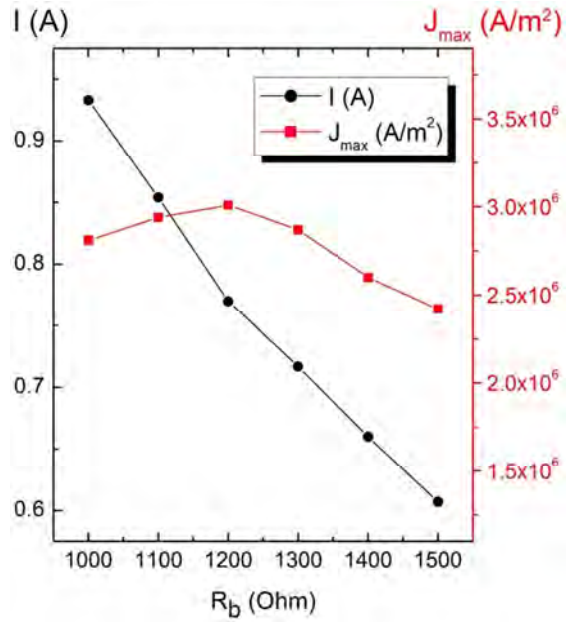

Figure 13. Cathode current and plasma arc peak current density vs. ballast resistance, at a flow rate of 22 L/min, t = 200 µs.

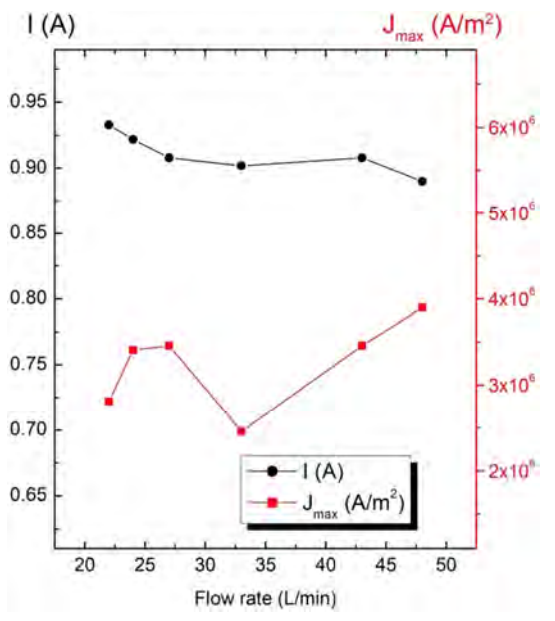

Figure 14. Cathode current and plasma arc peak current density vs. flow rate, at a ballast resistance of 1000 Ohm, t = 200 µs.

3.3. Plasma density, electron and gas temperature

The plasma arc "glides" along the circumference of the outlet, with the gas flow. In figure 15, the arc elongation is visualized. The arc ignites as a thin, straight plasma column, and is fully initialized at about 100 µs (figure 15a). After 1 complete revolution, which takes about 300 µs at a flow rate of 22 L/min, the arc starts to bend, and slightly elongate, crawling to the outer edge of the reactor. In figure 16, the arc movement is visualized, by showing snapshots of the plasma density as isosurfaces, at six different times, viewed from the top of the reactor, including the artificial heating function (first snapshot). The second and last snapshot of figure 16 correspond to figure 15a and 15b, respectively. The plasma density is in the order of 10^{21} m^{-3}, which is within the expected range for a gliding arc in argon at atmospheric pressure [1, 3, 4, 21]. It remains constant over time, and does not change significantly with flow rate. It is interesting to note that the arc at first tends to glide between the cathode center and the output nozzle edge (anode), where the electric field is slightly higher (see figure 10). The arc slowly crawls along the outlet wall, and after several revolutions, it stabilizes in the reactor center, attached to the outer edge of the outlet, and it remains there, swirling in a quasi-stationary state (figure 15b). A detailed animation of the arc movement is available in the supporting information of this paper.

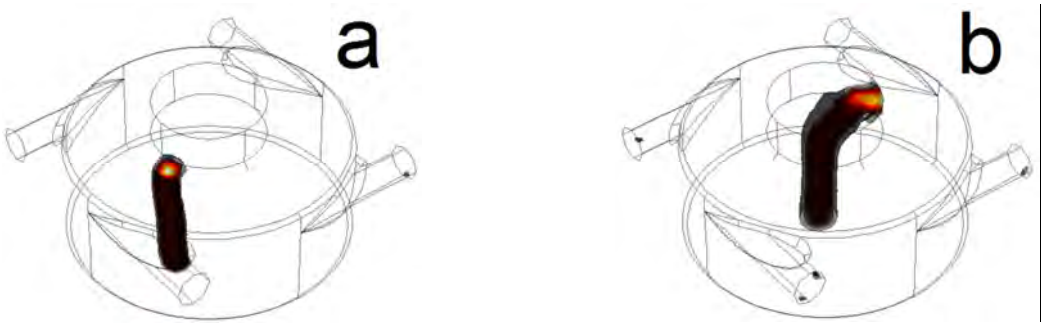

t = 100 µs. t = 1.1 ms.

Figure 15. Arc evolution over time, view of semi-transparent isosurfaces of plasma density. The arc ignites as a straight plasma column attached to the outlet edge (a). It crawls to the outer edge and stabilizes at the reactor center (b). Gas flow rate - 22 L/min, Rb = 1000 Ohm, current - 930 mA.

As is clear from figure 16, the arc gliding process is rather smooth and uninterrupted in our simulations. In reality, the arc movement is much more complex and spontaneous. Two reasons may account for the observed behavior. In the model, the cathode and the anode have perfectly flat, even surfaces. These surfaces are usually not completely smooth, and feature some microscopic bumps, scratches and lines, which create higher electric fields at certain points, causing the arc erratic behavior. Moreover, as the fluid flow is turbulent, small oscillations of the flow velocity will bend and deform the arc more significantly in a real-case experiment. However, these processes are very difficult to study in the present model, as a complex parameterization of the electrode surface would be required, and accordingly, a much finer discretization mesh at these surfaces. Furthermore, a finer mesh and turbulence modelling with a complete Navier-Stokes formulation would also be necessary for the gas in order to describe the turbulent eddies in the flow, and how they affect the arc movement, and shape. This is beyond the scope of the present study.

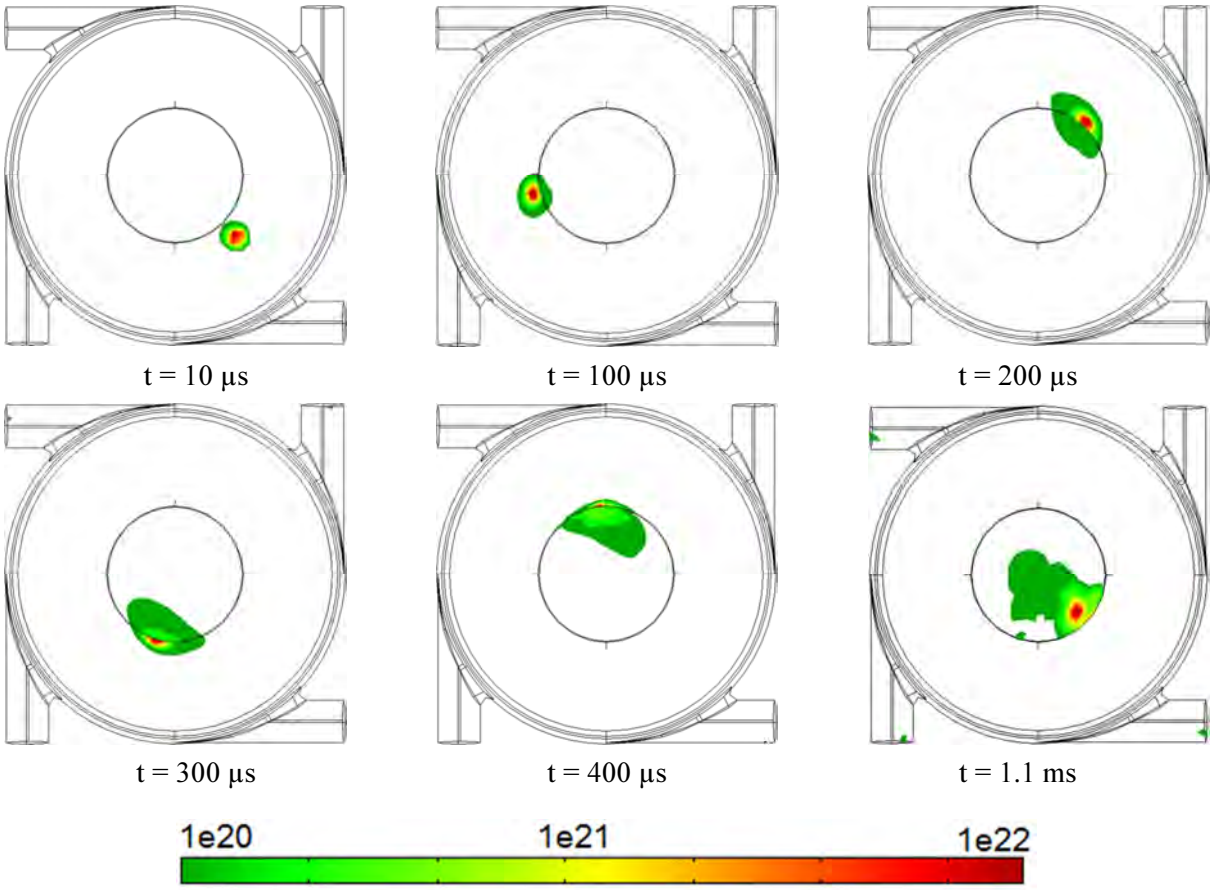

Figure 16. Plasma density (in m^{-3}), top view of several semi-transparent isosurfaces (different colour corresponds to different value). The plots are at different timeframes. The flow rate is 22 L/min and the current is 930 mA.

It is difficult to estimate the arc movement speed, as there are many effects that may alter it. First, the arc is attached to the electrodes, and more specifically, to the points with highest reduced electric field (E/n) magnitude, i.e. the sharp edges. Second, the flow velocity differs along the arc axis, and is very low near the electrodes. Third, the change in gas viscosity due to gas temperature may also influence the arc movement. In a real-case scenario, the electrode surface will also affect the arc movement, which would be much more erratic and spontaneous. Furthermore, the flow velocity varies across the arc body at its later development, so not all parts of the arc move with exactly the same velocity as the gas flow. We do not consider the thermal balance for the electrodes (as for the entire walls), which omits effects such as arc “anchoring”, again, due to computational limitations.

The spatial distributions of the gas and electron temperature are shown in figure 17 and figure 18 respectively, in a vertical cut plane through the reactor center and the arc. As is obvious from figure 17, the gas near the side walls of the reactor remain cool (300 K) due to the direction of the flow. The arc spins in the reactor center. Indeed, due to the characteristics of the RVF (figure 6), the mass transfer takes place from the walls to the center, effectively insulating the plasma from the sides.

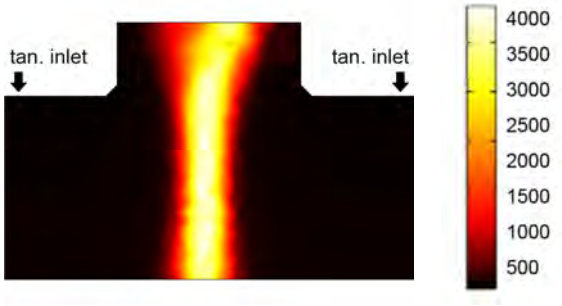

Figure 17. Gas temperature distribution in the reactor, for a gas flow rate of 22 L/min and a cathode current of 0.93 A, after 1.5 ms.

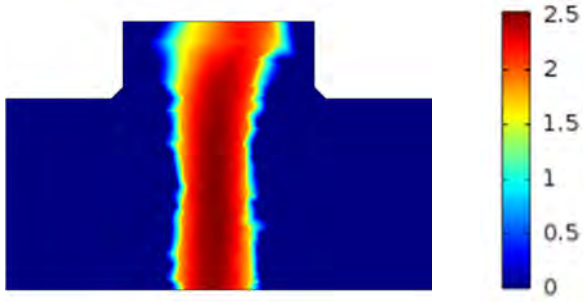

Figure 18. Electron temperature distribution in the reactor, for a gas flow rate of 22 L/min and a cathode current of 0.93 A, after 1.5 ms.

As a result, the high temperature gas is confined in the reverse-vortex, and therefore, the plasma thermal insulation is nearly perfect. This is in agreement with earlier studies on the RVF [11]. The maximum gas temperature, in the arc body, is slightly above 4000 K at the given conditions. The electron temperature within the arc body (figure 18) is in the order of 2.5 eV, which is rather high for a gliding arc discharge, because in literature values around 1 eV are typically reported [1, 3]. This might be explained by the simplifications, defined in the model.

In figures 19 and 20, the arc plasma density, the electron temperature and gas temperature are plotted at different values of cathode current and gas flow rate, respectively. For figure 19, the results are generated by applying a time-dependent function to the ballast resistor, which increases its value over time. The function is activated after t = 1.1 ms., where the discharge reaches a quasi-stationary state of operation, i.e. the arc characteristics do not change anymore and it's rotation is stabilized in the reactor center (see figure 15). The resistance value changes with a much slower rate compared to the time for settlement of the plasma-gas parameters, so the values are the same as if running the model from the beginning, with a fixed resistance value. This approach allows us to obtain continuous results while saving computing time. The plasma density demonstrates a slight change in the given range of conditions, with values in the arc center in the order of $0.8 \times 10^{21} - 2 \times 10^{21}$ m^{-3} . The electron temperature exhibits almost no change, with values of 2.5 – 2.6 eV. The gas temperature clearly rises with increasing cathode current. Furthermore, increasing the flow rate leads to a lower gas temperature in the arc (figure 20). This can be explained by the increased mass flow in the reactor.

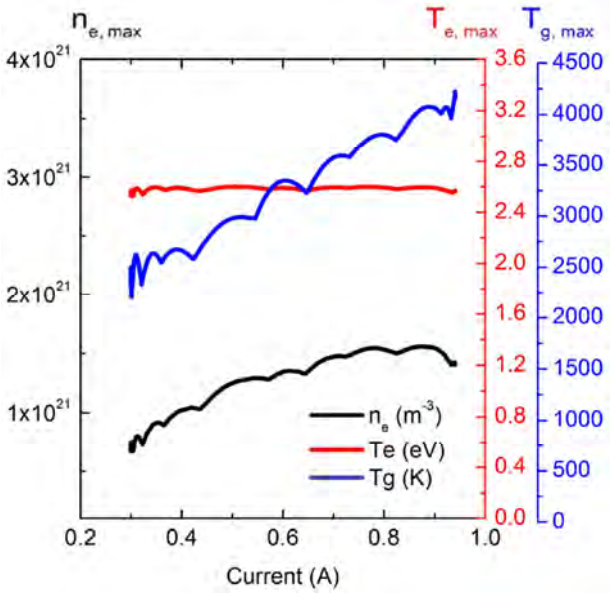

Figure 19. Plasma density, electron temperature and gas temperature vs. cathode current, at a gas flow rate of 22 L/min, quasi-stationary state at 1ms.

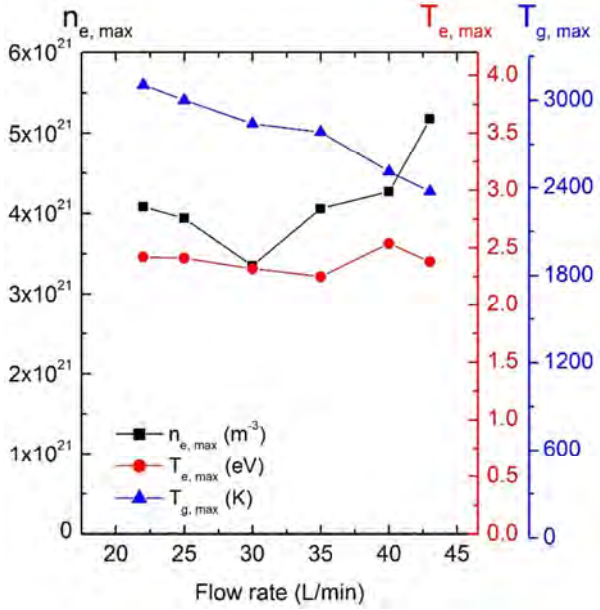

Figure 20. Plasma density, electron temperature and gas temperature vs. flow rate, at a cathode current of 900 mA and t = 200 µs.

At flow rates above 45 L/min, the gas temperature becomes relatively low and thus there is no arc contraction, i.e. the plasma channel becomes very wide, filling the whole domain, i.e. it is not an arc anymore. At flow rates below 20 L/min, the gas temperature becomes too high for the simulation, i.e., the finite mesh is unable to handle the strong temperature gradients, and thus, the computation fails. The obtained values for the arc temperature are comparable with some earlier studies on gliding arc discharges, with and without RVF stabilization [3, 4].

4. Conclusion

In the present paper, the physics of a RVF gliding arc reactor is simulated by means of fluid plasma modelling. The properties of the gas flow are obtained using the k-ε RANS turbulent model, and the results correspond well with previous studies on RVF gliding arc reactors [9, 10]. The plasma itself is modelled by means of a quasi-neutral model with a reduced reaction set. The calculated current density corresponds well to the theory and practice of low current atmospheric pressure discharges [1, 3, 4]. The calculated values for plasma density and gas temperature are comparable with experimental and numerical data on gliding arc plasma reactors, with and without RVF stabilization [3, 4, 21]. Indeed, in [3], values were reported for a plasma density of $10^{18} – 10^{19}$ m^{-3}, a gas temperature of 1100 – 2600 K, and an electron temperature of 1 eV for a conventional, lower-current gliding arc reactor operating at 130 mA . In [11], a reverse-vortex was simulated using the RSM (Reynolds stress model) turbulent model with a cylindrical shape to act as a heat source for the reactor. The thermal insulation behavior was very similar to our case. In [21], plasma densities of $10^{22} – 5x10^{22}$ m^{-3} were reported for a conventional high-power argon gliding arc operating at 68 W, which is very close to the values obtained in the presented model. Certainly, it is not easy to compare different gliding arc setups with different reactor geometries. Our calculated electron temperature is quite high compared to most experimental data for a GA in argon, although it is not dramatically higher, i.e. 1 eV in [3] vs. 2-2.5 eV in our model.

Our calculations also indicate that the arc voltage changes with gas flow rate. The arc gas temperature also depends on the total power deposition (or cathode current) and the flow rate, while the plasma density and electron temperature remain constant after a stable state of the arc is reached. Furthermore, the arc movement is visualized, and although it might not be 100% accurate because of model limitations, it can be concluded that the plasma arc clearly stays well insulated from the side walls due to the gas flow. Thus, the walls are almost perfectly insulated from the plasma, protecting them from the high temperature, and improving the efficiency of the reactor.

The computational time of the model is reasonable, with the stationary study for the gas flow computed within 2 hours, and about 100 μs of the time-dependent plasma model computed within 24 hours on an Intel i7-3820 (4 cores at 3.7 GHz) CPU with 64 GB of RAM.

The model still exhibits some limitations. First, the mesh density of 150,000 elements for the entire model, with element size of 0.3-0.7 mm, should be considered as a lower limit for adequate calculations. However, a denser mesh would simply take too much time to compute for the given time frame. For this reason, the calculated arc shape and arc movement are only approximate. Second, the reaction set is reduced to a minimum, which allows computation of the model without significantly hampering the accuracy. This approach may be suitable for argon, but for other gases envisaged for further investigation, such as CO_2, it would represent a significant problem. Indeed, for the application of CO_2 conversion, a more detailed plasma chemistry set would have to be incorporated, dramatically increasing the calculation time [28, 29, 30]. Third, the quasi-neutral assumption of the model leaves out the possibility to study the Debye sheaths at the boundary areas and the electrodes, which makes the model reliable only with respect to the properties of the plasma column. Also, the reactor shape does not correspond to the features of a real device, but only to a simplified description of a reverse-vortex tube [1], again, for the sake of optimizing the computation time. Other methods for refining, such as adaptive mesh generation were explored, but the resulting computation time was too long.

Finally, the lack of concrete experimental and other simulation data for RVF gliding arc reactors makes it difficult to validate our model. This reactor type is relatively new, and is only recently gaining interest in the fields of plasma gas conversion, plasma fuel enhancement, and plasma surface processing. We hope that more experimental data will become available, allowing us to better validate our model. As a final remark, this study proves that problems, which are essentially 3-dimensional in nature, are now within the grasp of modern plasma modelling techniques.

6. Acknowledgements

This research was carried out in the framework of the network on Physical Chemistry of Plasma-Surface Interactions - Interuniversity Attraction Poles, phase VII (http://psi-iap7.ulb.ac.be/), and supported by the Belgian Science Policy Office (BELSPO), and it was also funded by the Fund for Scientific Research Flanders (FWO). Grant number: 11U5316N.

7. References

[1] A Fridman, *Plasma Chemistry*, p. 187-207, Cambridge University Press, New York, US, 2008

[2] X Tu, J C Whitehead, Plasma dry reforming of methane in an atmospheric pressure AC gliding arc discharge: Co-generation of syngas and carbon nanomaterials, Int. J. Hydrogen Energy, **39**, 9658-9669, 2014

[3] A Czernichowski, H Nassar, A Ranaivosoloarimanana, A Fridman, M Simek, K Musiol, E Pawelec, L Dittrichova, Spectral and electrical diagnostics of gliding arc, Acta Physica Polonica A, **89**, 595-603, 1996

[4] A El-Zein, G El-Aragi, M Talaat, A El-Amawy, Discharge characteristics of gliding arc plasma reactor with argon/nitrogen, Journal of Advances in Physics, 7(1), 1316-1323, 2015

[5] A Fridman, A Gutsol, S Gangoli, Characteristics of Gliding Arc and Its Application in Combustion Enhancement, J. Prop. Power, **24**, 1216-1228, 2008
[6] A Indarto, D Yang, J Choi, H Lee, H Song, Gliding arc plasma processing of CO_2 conversion, J. Hazard. Mat., **76**, 025110, 2005
[7] J Liu, H Park, W Chung, D Park, High-Efficient Conversion of CO_2 in AC-Pulsed Tornado Gliding Arc Plasma, Plasma Chem. Plasma Process., **09**, 2015, DOI: 10.1007/s11090-015-9649-2
[8] A Indarto, Jae-Wook Choi, Hwang Lee and Hyung Keun Song, Conversion of CO_2 by Gliding Arc Plasma, Env. Eng. Sc., **23**, 1033-1043, 2006
[9] T Nunnaly, K Gutsol, A Rabinovich, A Fridman, A Gutsol, A Kemoun, Dissoaciation of CO_2 in a low current gliding arc plasmatron, J. Phys. D: Appl. Phys, **44**, 274009, 2011
[10] C Kalra, Y Cho, A Gutsol, A Fridman, Gliding arc in tornado using a reverse vortex flow, Rev. Sc. Instrum., **76**, 025110, 2005
[11] A Gutsol, J A Bakken, A new vortex method of plasma insulation and explanation of the Ranque effect, J. Phys. D: Appl. Phys., **31**, 704-711, 1998
[12] O A Nedybaliuk, V Ya Chernyak, S V Olszewski and E V Martysh, Dynamic Plasma-Liquid System with Discharge in Reverse Vortex Flow of "Tornado" Type, Int. J. Plasma Env. Sc. & Tech., **5**, 20-24, 2011
[13] C S Kalra, M Kossitsyn, K Iskendrova, A Chirokov, Y I Cho, A Gutsol, A Fridman, Electrical discharges in the Reverse Vortex Flow – Tornado Discharges, Electronic Proceedings of 16th International Symposium on Plasma Chemistry, Taormina, Italy, June 22-27, 2003, ISPC-565
[14] A F Gutsol, J Larjo and R Hernberg, Reverse-Flow Swirl Radio-Frequency Induction Plasmatron, Teplofizika Vysokikh Temperatur, **39**, 187-197, 2001
[15] A Gutsol, Gaseous flame in the reverse-vortex, Matematicheskoe modelirovanie, **11**-6, 1999
[16] St Kolev, A Bogaerts, A 2D model for a gliding arc discharge, Plasma Sources Sci. Technol., **24**, 015025, 2015
[17] J H Ferziger, M Peri'c, *Computational Methods for Fluid Dynamics 3rd ed.*, p. 265-306, Springer-Verlag, Germany, 2002
[18] D C Wilcox, Turbulence Modeling for CFD 3rd ed., DCW Industries Inc., US, 2006
[19] W Rodi, Comparison of LES and RANS calculations of the flow around bluff bodies, J. Wind Eng. Ind. Appl., **69-71**, 55-75, 1997
[20] A Gleizes, J J Gonzalez and P Freton, Thermal plasma modelling, J. Phys. D: Appl. Phys., **38**, R153-R183, 2005
[21] X Tu, J Gallon, J C Whitehead, Electrical and optical diagnostics of atmospheric pressure argon gliding arc plasma jet, 30th ICPIG, Belfast, Northern Ireland, UK
[22] St Kolev, SR Sun, HX Wang, A Bogaerts, Reliability of a quasineutral plasma model for gliding arc discharge modelling, paper in preparation
[23] B Parent, M Shneider and S Macheret, Sheath governing equations in computational weakly-ionized plasmadynamics, J. Comp. Phys., **232**, 234-251, 2013
[24] P Rosenau and Eli Turkel, Ambipolar Diffusion in a Multi-Species Medium, Physica Scripta., **31**, 207-209, 1985
[25] Comsol 5.0, Plasma Module User's Guide, https://www.comsol.com
[26] BIAGI-v7.1 database, www.lxcat.laplace.univ-tlse.fr; Transcribed from SF Biagi's Fortran code MAGBOLTZ,http://consult.cern.ch/writeup/magboltz
[27] A Gutsol, The Ranque effect, Physics – Uspekhi **40**(6), 639-658, 1997
[28] T Kozak, A Bogaerts, Splitting of CO_2 by vibrational excitation in non-equilibrium plasmas: a reaction kinetics model, Plasma Sources Sci. Technol., **23,** 045004, 2014
[29] T Kozak, A Bogaerts, Evaluation of the energy efficiency of CO_2 conversion in microwave discharges using a reaction kinetics model, Plasma Sources Sci. Technol, **24**, 015024, 2015
[30] R Snoeckx, R Aerts, X Tu, A Bogaerts, Plasma – Based Dry Reforming: A Computational Study Ranging from the Nanoseconds to Seconds Time Scale, J. Phys. Chem. C., **117**, 4957-4970, 2013